Author(s): Ryabchun, Alexander; Lancia, Federico; Chen, Jiawen; Morozov, Dmitry; Feringa, Ben L.; Katsonis, Nathalie

Title: Helix Inversion Controlled by Molecular Motors in Multistate Liquid Crystals

Year: 2020

Version: Published version

Please cite the original version:

Ryabchun, A., Lancia, F., Chen, J., Morozov, D., Feringa, B. L., & Katsonis, N. (2020). Helix Inversion Controlled by Molecular Motors in Multistate Liquid Crystals. Advanced Materials, 32(47), Article 2004420. https://doi.org/10.1002/adma.202004420

Helix Inversion Controlled by Molecular Motors in Multistate Liquid Crystals

Alexander Ryabchun, Federico Lancia, Jiawen Chen,* Dmitry Morozov, Ben L. Feringa,* and Nathalie Katsonis*

Unravelling the rules of molecular motion is a contemporary challenge that promises to support the development of responsive materials and is likely to enhance the understanding of functional motion. Advances in integrating light-driven molecular motors in soft matter have led to the design and realization of chiral nematic (cholesteric) liquid crystals that can respond to light with modification of their helical pitch, and also with helix inversion. Under illumination, these chiral liquid crystals convert from one helical geometry to another. Here, a series of light-driven molecular motors that feature a rich configurational landscape is presented, specifically which involves three stable chiral states. The succession of chiral structures involved in the motor cycle is transmitted at higher structural levels, as the cholesteric liquid crystals that are formed can interconvert between helices of opposite handedness, reversibly. In these materials, the dynamic features of the motors are thus expressed at the near-macroscopic, functional level, into addressable colors that can be used in advanced materials for tunable optics and photonics.

Dr. A. Ryabchun, Dr. F. Lancia, Prof. N. Katsonis
Stratingh Institute for Chemistry
University of Groningen
Nijenborgh 8, Groningen 9747 AG, The Netherlands
E-mail: n.h.katsonis@rug.nl

Dr. J. Chen
Institute of Electronic Paper Displays
South China Academy of Advanced Optoelectronics
South China Normal University
Guangzhou 510006, China
E-mail: j.chen@m.scnu.edu.cn

Dr. D. Morozov
Department of Chemistry and Nanoscience Center
University of Jyväskylä
PO Box 35, Jyväskylä 40014, Finland

Prof. B. L. Feringa
Center for Systems Chemistry
Stratingh Institute for Chemistry
University of Groningen
Nijenborgh 4, Groningen 9747 AG, The Netherlands
E-mail: b.l.feringa@rug.nl

The ORCID identification number(s) for the author(s) of this article can be found under https://doi.org/10.1002/adma.202004420.

Artificial molecular motors and switches are called to contribute in setting materials in motion.[1–5] Ongoing efforts to enable transmission of motion and allow molecular machines to work at larger length scales involve their integration in hydrogels,[6–8] self-assembled monolayers,[9] artificial muscles,[10,11] and polymer materials.[12] The long-range organization and fluidity of liquid crystals accounts for their high responsiveness to small changes in molecular structure or composition, with a special sensitivity to changes in chirality.[13] Therefore, liquid crystals constitute an effective host medium for molecular motors and switches.[14–16] Chiral molecular switches can drive dynamic helix inversion in liquid crystals,[17–24] and artificial molecular motors also induce the formation of chiral nematic liquid crystals that respond to light with large changes in pitch and in the orientation of the helical axis, usually also with chiral inversion at the photostationary state.[25,26] Motor-doped cholesteric liquid crystals have supported the discovery of rotating surfaces,[27–29] supramolecular vortices,[30] swimming[31] and reconfigurable chiral droplets,[32] and adaptive optical materials.[33,34] Notably, while being at the forefront of light-responsive and adaptive materials, to date motor-doped liquid crystals have been used primarily for their ability to convert from one helix to another, reversibly. These earlier studies have involved "second generation" motors, for which only the expression of two states was possible, because only two isomers of these motors can be distinguished at room temperature.[35,36] Here, we report the motion of the so-called "first generation" molecular motor in liquid crystals, in a cyclic behavior that involves four distinct isomeric states. These motors induce light-responsive helices in liquid crystals, which readily undergo photomodulation of the liquid crystal phase, including helix inversion. While multistate liquid crystal helices can be designed by mixing chiral dopants,[37,38] using a single chiral dopant—for example, by incorporating multiple light-switchable units,[14,39,40] is a better option as this prevents solubility issues and offers better options for rational design, as predictions on the pitch formed by a mixture of chiral dopants lack reliability, particularly at larger concentrations.

Key to the design of molecular motors that are able to drive multistate and photoinvertible helices is that each of the motor states displays a distinctively different shape, i.e., either
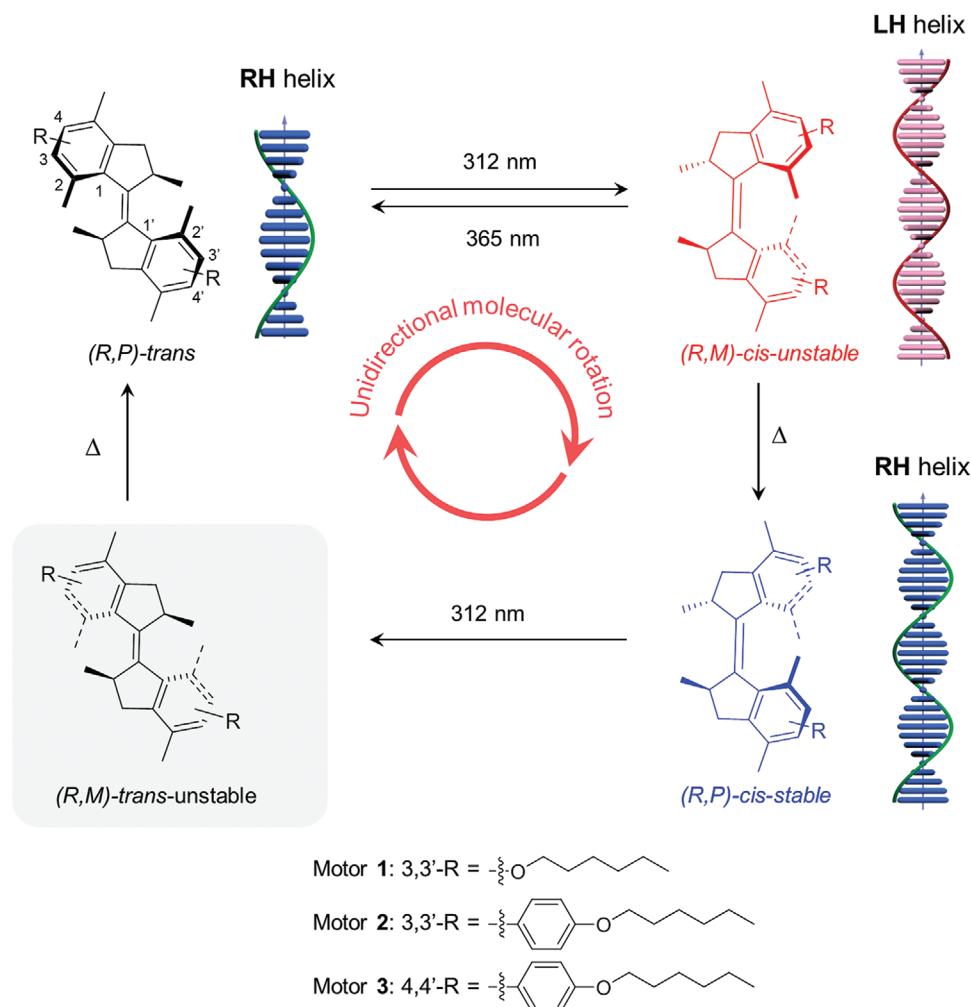
Figure 1. Four steps rotary cycle of a "first generation" molecular motor in which the bottom and upper halves are identical. Only the (R)-enantiomer is shown. The (R,M)-trans-unstable isomer is not stable under ambient conditions. RH stands for right-handed and LH stands for left-handed.

an elongated "rod-like" shape or a marked helical "V-shape" (**Figure 1**). This feature is present in "first generation" motors, the structure of which is symmetric and includes the recognizable structural motif of a "stiff-stilbene."[41–45] The bottom and the upper halves of the motor are identical and the position of the substituents at the motor core is intended to maximize the shape anisotropy of all the isomers; typically the (R,P)-trans form is elongated, whereas the (R,M)-cis-unstable and the (R,P)-cis-stable have helical shapes of opposite handedness.

In solution, illuminating the (R,P)-trans-stable isomer of all three motors (λ = 312 nm) initiates the trans-to-cis isomerization of the central double bond. The photoisomerization results in the formation of the (R,M)-cis-unstable isomer that features steric hindrance related to the (M)-helicity. The (R,M)-cis-unstable isomer then undergoes an energetic downhill thermal helix inversion to yield the (R,P)-cis-stable isomer. The thermal helix inversion is irreversible and confers unidirectionality to the motor rotation. The handedness of the molecule is reversed again from M to P during thermal relaxation. Alternatively, when the cis-stable isomer is illuminated with λ = 312 nm light, the rotation cycle proceeds via initial formation of the

trans-unstable form followed by thermal helix inversion to the trans-stable isomer (Figure 1). Notably, the (R,M)-trans-unstable isomer cannot be detected at room temperature.

NMR investigations of motors **1–3** in solution reveal a (cis-unstable/trans) photoconversion ratio of 72/28, 87/13, and 77/23, respectively (Figures S13–S15, Supporting Information). After illumination, the samples were kept in the dark at 50 °C overnight, to promote cis-unstable to cis-stable helix inversion, as evidenced by up-field shifts of all NMR signals (Figures S13–S15, Supporting Information). The ratios of cis-stable/trans are equivalent to the ratios of cis-unstable/trans for all motors, which indicates that thermal E–Z isomerization does not happen spontaneously and therefore confirms unidirectionality of the motor rotation.

In solution, the rotary cycle of **1–3** was also followed by UV/vis absorption, fluorescence, and circular dichroism (CD) spectroscopies (**Figure 2**). UV/vis absorption shows that the band corresponding to the trans-state is the most blueshifted. The cis-unstable-state shows the main absorbance band substantially at a longer-wavelength region (λ > 355 nm). The absorption spectra of all three isomers of motor **3** are redshifted
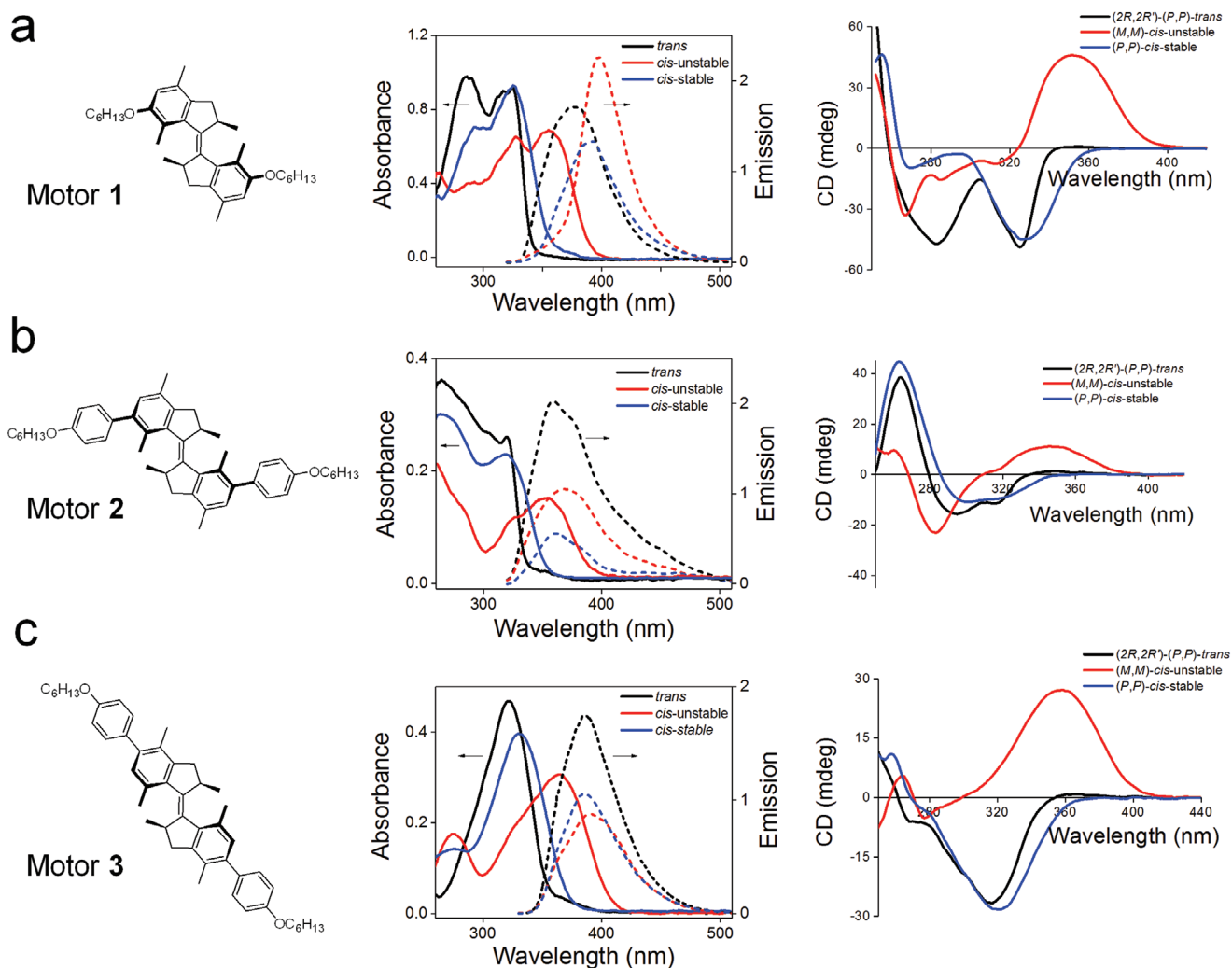
ADVANCED
SCIENCE NEWS
www.advancedsciencenews.com

ADVANCED
MATERIALS
www.advmat.de

Figure 2. a–c) Structure, absorbance, emission, and circular dichroism spectra of motors (R,P)-**1** (a), (R,P)-**2** (b), and (R,P)-**3** (c). The spectra were recorded in DMSO at room temperature. The *cis*-unstable state was obtained by irradiating the *trans*-state with UV light (λ = 312 nm), until a photo-stationary state was reached. For the emission spectra, the excitation wavelengths were λ = 300 nm for motors **1** and **2**, and λ = 320 nm for motor **3**.

compared to those of motor **1** and motor **2**, likely because the conjugation between the two halves of motor **3** is enhanced by the alkyloxy-substituents in *para*-position.

Motors **1**–**3** are also fluorescent, with emission from the *trans*-state being more intense than from both *cis*-states (Figure 2a–c). In contrast with the behavior of motor **1**, the fluorescence spectra of motors **2** and **3** are not modified substantially during the rotation, likely due to additional delocalization caused by a larger π–π conjugated system. CD spectroscopy of the motors shows that the *trans*- and *cis*-stable-states have the same helicity in solution. Upon irradiation with UV light (λ = 312 nm), CD signal inversion indicates helix inversion.

A small amount of enantiomerically pure motor (typically 1 wt%) was incorporated as chiral dopant in an (achiral) nematic liquid crystal. The pitch that is formed is described by a phenomenological parameter called the helical twisting power (HTP; see Equation (1))

$$HTP = P^{-1}/Cee \tag{1}$$

where P is the cholesteric pitch, C is the concentration of motor dopant, and ee is the enantiomeric excess. By convention, the twisting power is positive for right-handed helices and negative for left-handed helices.

A nematic liquid crystal composed of molecules that do not absorb light at λ = 312 nm has been used as a host (ZLI-1132). First generation motors also induce a twist in other nematic hosts (Tables S1 and S2, Supporting Information), however, here, we focus on ZLI-1132 due to its transparency at the working wavelength of molecular motors. The helical twisting powers of all (R,P)-enantiomers were determined by the Grandjean–Cano wedge cell method,[46] revealing that (R,P)-**1** motor induces left-handed helices in both its *trans*- and *cis*-unstable forms (**Table 1**), however the HTPs are low which indicates that the chirality transfer is moderate. By contrast, the helical twisting power of (R,P)-**2** is large, and comparable to those of the "second generation" molecular motors.[29] (R,P)-*trans*-**3** and (R,P)-*cis*-stable-**3** induce a left-handed helix, whereas (R,M)-*cis*-unstable-**3** induces a right-handed helix

Table 1. Values of helical twisting powers ($HTP_{wt\%}$ in μm^{-1}) for (R)-motors **1**, **2**, and **3**, in all three states that are involved in the motor cycle.

Motor	trans-Isomer	PSS[a]	cis-Unstable-isomer[b]	cis-Stable-isomer
1	−26.4	−42.3/−44.9	−48.6	+25.3
2	+4.8	−77.6/−87.4	−88.9	+75.5
3	−49.9	−7.8/−9.7	+4.8	−17.4

[a]PSS refers to cis-unstable isomer of the motor, which was generated in situ starting either from the trans-state (numbers on the left) or from the cis-stable-state (numbers on the right) by irradiating with light at $\lambda = 312$ nm; [b]This HTP value was calculated based on the measured composition of the photostationary state at $\lambda = 312$ nm.

(HTP = +4.8 as calculated from the composition of the photostationary state).

Axial chirality is associated with the stilbene-like helical shape of the molecular motor, in which two benzyl rings are connected through an overcrowded alkene. The helical twisting powers of the motors in a nematic liquid crystal are shown in Table 1. Their values can be rationalized by comparing the methyl-related central chirality with the stilbene-like axial chirality of the molecular motor. In the cis-forms of motors **1** and **2**, the stilbene-like asymmetry predominates and is likely responsible for the large values of helical twisting powers (Figures S16 and S17, Supporting Information). Notably, the elongation of the rigid core at the 3,3′-position in motor **2** enhances the

stilbene-like helical shape, and therefore, the values of HTP are double than those associated with motor **1** (Table 1). Less intuitively, elongation of the core at the 4,4′-positions reduces the helical shape of the stilbene-like feature (Figure S18, Supporting Information), and the resulting helical twisting power thus relies mainly on the expression of the methyl-related chirality. The (S,M)-enantiomers of motors **1**–**3** demonstrate opposite behavior compared to the (R,P)-enantiomers, in terms of chirality transduction (Table S2, Supporting Information). Both enantiomers of all three motors can thus induce dynamic helix inversion, reversibly (**Figure 3**a) with the highest range of HTP variation achieved by molecular rotation of motor **2** (ΔHTP > 160). In contrast with Table 1 that features the HTP values of chemically pure motors, Figure 3a and Table S3 in the Supporting Information feature all practically important variations of helical twisting power that can be reached photochemically and upon heating.

The stability of cis-unstable forms of the motors in a nematic liquid crystal was estimated by doping the liquid crystal with 1 wt% of motor in the trans form. The cis-unstable form was generated in situ by using illumination with $\lambda = 312$ nm light, and the relaxation of cis-unstable- to cis-stable was investigated by following spectral changes (Figure 3b; Figure S19, Supporting Information). With a half-life time of ≈113 h, cis-unstable-**1** is significantly less stable than both cis-unstable-**2** (824 h) and cis-unstable-**3** (955 h) in the liquid crystal. Notably the cis-unstable forms of all three motors have considerably longer
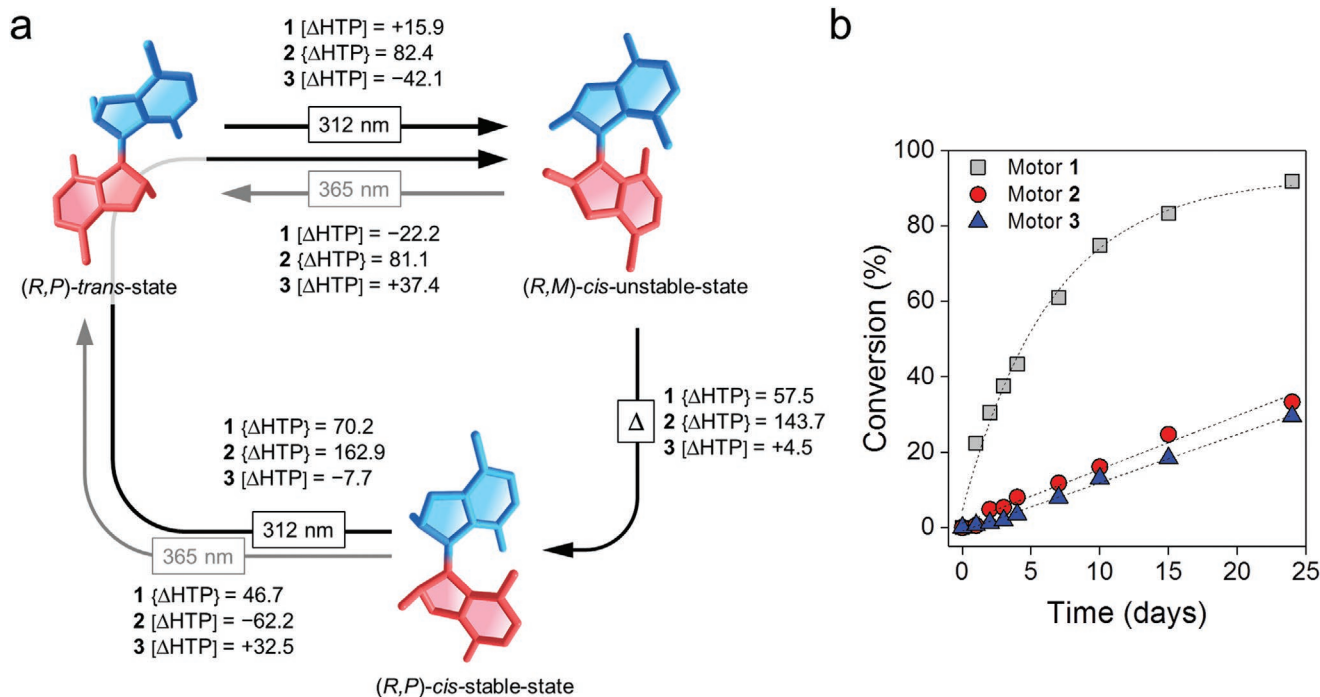

Figure 3. a) Representation of the motor cycle and variation of helical twisting power associated with each step. The transformations of the (R,P)-motor are associated with large changes in the helical twisting power (HTP). The notation [ΔHTP] indicates that the HTP changes without helix inversion. Positive and negative values correspond to increase and decrease in HTP, respectively. The notation {ΔHTP} indicates that the change in helical twisting power is associated with helix inversion. The handedness of the liquid crystal helix can be selectively addressed by irradiation at $\lambda = 312$ nm, or at $\lambda = 365$ nm, or by heat. b) Kinetics of relaxation from the cis-unstable-state to the cis-stable-state of motors **1**–**3** in a liquid crystalline environment. The thermal isomerization was followed by UV–vis spectroscopy at room temperature in the dark. The cis-unstable state was generated inside home-made quartz cells by irradiating the trans-isomer at $\lambda = 312$ nm. This data shows that the motor-based liquid crystals retain their properties for days and months when the motors are in their "unstable" state, however, they can be turned back or forth by UV exposure or mild heating up.
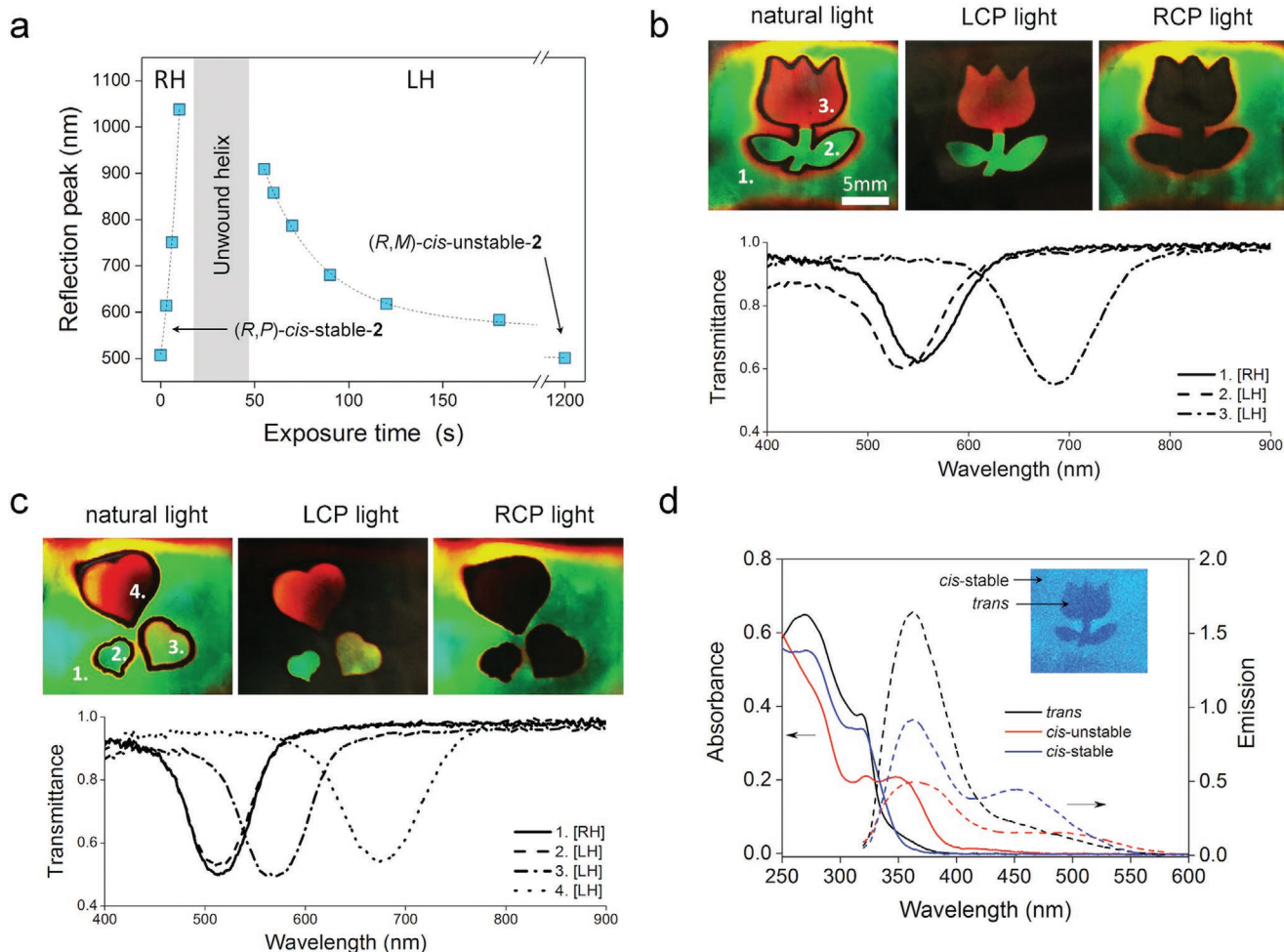
Figure 4. Photopatterning multiple and circularly polarized reflection colors in a single material. a) Evolution of helix pitch and handedness of a liquid crystal (ZLI-1132) doped with motor *cis*-stable-**2** (4 wt%) upon exposure to UV light (λ = 300 nm). The notations RH and LH indicate right- and left-handed cholesteric helices, respectively. b,c) The thin cholesteric layers with recorded patterns were visualized under natural (nonpolarized) light and under left- and right-circular polarized light (LCP and RCP, respectively). Samples were irradiated at λ = 300 nm, through a mask. The reflection from the cholesteric liquid crystal can be visualized selectively by using circular polarizers, while irradiating with natural (nonpolarized) light allows visualizing of both RH and LH reflection colors. The transmission spectra corresponding to the different colors are provided in the panel below. d) Absorbance (solid lines) and fluorescence (dashed lines) spectra of liquid crystal film (ZLI-1695) doped with motor *cis*-stable-**2** (1 wt%). The inset shows a fluorescence image for irradiation through a mask with λ = 365 nm light (the excitation wavelength being λ = 312 nm). The motor is in the *trans*-state inside the flower pattern, while the outside of the flower pattern is in the *cis*-stable state. These two areas are distinguishable by their fluorescence. The dimension of the sample is 2 × 2 cm.

half-life times in the liquid crystals, compared to those in the isotropic solution (typically for **1** $t_{1/2}$ ≈113 h in the liquid crystal and $t_{1/2}$ ≈18.6 h in solution; see Figure S20 in the Supporting Information), which indicates that the *cis*-motor is stabilized by interaction with the liquid crystal.

The system allows photopatterning of multiple stable colors in the same thin film of liquid crystal, because it provides the expression of different chiral states that can be addressed selectively. The color reflected by liquid crystal helices (λ_o) is defined by the pitch of the helix (Equation (2))

$$\lambda_o = nP \tag{2}$$

where n is the average refractive index, and P is the cholesteric pitch. Moreover, the reflected light is circularly polarized,

therefore optical information can be encoded independently by the handedness of the helices and color.

We prepared a thin film of right-handed material incorporating 4 wt% of *cis*-stable-**2**, in order to demonstrate the optical recording opportunities offered by this motor design. This liquid crystal system reflects green light selectively with a right-handed circular polarization. Illumination at λ = 300 nm first unwinds the helix, as seen in the redshift of the reflection band, followed by an inversion of chirality and a subsequent blueshift due to the rotation of the motor from *cis*-stable- to the *cis*-unstable-isomeric form (**Figure 4**a). The helix inversion proceeds through the formation of completely unwound state where the twisting powers of all the motor isomers compensate each other. Overall, the multistate responsive helices realized by the molecular motors are associated with a wide

spectral range of reflection colors, and their handedness can be controlled independently. As soon as the irradiation is stopped, the reflection color of the sample is fixed because the isomeric composition of the material is stable in time.

Spatial color resolution and consequently optical information recording can be achieved by engineering the cholesteric helices locally, and therefore complex optical patterns can be designed simply by irradiating a sample through a mask (Figure 4). Figure 4b shows a flower pattern on a liquid crystal film doped with 4 wt% of *cis*-stable-**2**. The body of the flower was patterned by irradiating a mask with UV light, until the irradiated liquid crystal helices reach a pitch associated to green and red reflection colors. Significantly, because of helix inversion, these green and red colors are produced by helices that have the opposite handedness than the initial material. Where areas with opposite chirality meet, a thin black border is visible that corresponds to the unwound helix. Observation of the flower pattern under circularly polarized light reveals the reflection colors in the patterns selectively (Figure 4b, middle and right panels)—in other words, colors formed by right-handed helices will be revealed only under right-handed circularly polarized light and, conversely, colors formed by left-handed helices will be revealed only under left-handed circularly polarized light. A variety of patterns can be designed (Figure 4c), however, their stability is limited to several hours because the motor diffuses laterally in the liquid crystals, which are essentially fluids. We envision that diffusion should not constitute a fundamental limitation for future developments towards optical information recording because liquid crystals can be stabilized by cross-polymerization or by using side-chain liquid crystal polymers.

The fluorescence of the *cis*-stable isomer significantly differs from that of the other isomers—an observation that is specific to the motors in a liquid crystal environment (Figure 4d for motor **2**; Figure S21 in the Supporting Information for motors **1** and **3**), and was not observed in solution. Because different isomers have different fluorescence characteristics, it becomes possible to encode fluorescent patterns in this material. The spatial distribution of isomeric forms of the motor can be followed visually, using fluorescence colors (inset in Figure 4d). On an image displaying different fluorescent colors, the *trans*-isomer of motor **2** emits in the ultraviolet, while the rest of the sample display emission in the visible spectral range inherent to initial *cis*-stable-state of motor **2**. As the polarization of the emitted light is determined by the handedness of the cholesteric helix,[47,48] it should become possible to switch the handedness of the emitted light, reversibly, provided that the emission spectrum of the motor overlaps with the position of the reflection band.

In conclusion, the multistep operation of molecular motors was converted into the multistep photoconversion of cholesteric helices, with three stable chiral states that can be addressed by light, selectively, and reversibly. The "first generation" molecular motors reveal good solubility and chemical stability in liquid crystals, and offer the opportunity to engineer multiple liquid crystal helices with light, with large changes in helical twisting power including helix inversion. Expressing the rotation cycle of these molecular motors to the near macroscopic level thus broadens the range of helix-based materials that can be engineered with light reversibly. As each state of "first generation" motors is associated with a different helical handedness, integrating these motors in liquid crystalline materials also reveals in a unique way how chirality is transmitted across length scales in dynamic supramolecular systems.

Experimental Section

Synthesis: Motors **1**–**3** were synthesized using McMurry and Suzuki couplings as key steps; detailed synthetic procedures, purification, and characterizations are reported in Scheme S1 and Figures S1–S12 in the Supporting Information.

Sample Preparation: Nematic liquid crystals ZLI-1132 and ZLI-1695 were purchased from Merck and used as received. The motor-doped cholesteric liquid crystals were prepared by dissolving the motor and nematic liquid crystal in dichloromethane, followed by solvent evaporation and drying in vacuum. Next, these materials were introduced by capillary into sandwich-like quartz cells or wedge-like cells. Nematic liquid crystal ZLI-1132 was always used as a host except in Figure 4d, where ZLI-1695 was used. The optical properties of the motors in liquid crystals were investigated in home-made quartz cells of 10 μm thickness. Unidirectional orientation of the liquid crystal was achieved by using alignment coatings.

Measurements: The polarized optical microscopy investigations were performed using a microscope BX51 (Olympus). The absorption and transmittance spectra were measured using a spectrometer HR2000+ (Ocean Optics).

Fluorescence measurements were performed using an LS55 (Perkin Elmer) spectrometer. As light sources for photo-optical studies, LEDs (Thorlabs) with wavelengths $\lambda = 300$ nm ($I \approx 2.7$ mW cm^{-2}) and $\lambda = 365$ nm ($I \approx 10$ mW cm^{-2}), and a mercury lamp (Spectroline) with a $\lambda = 312$ nm filter ($I \approx 2.5$ mW cm^{-2}) were used. The intensity of the light was measured using a power meter PM-100D (Thorlabs).

HTP values were determined by the Grandjean–Cano method. For practical guidelines, see ref. [30]. The handedness of the cholesteric liquid crystals was determined by exploiting a rotatable analyzer in the Grandjean–Cano wedge cell configuration.[49] The wedge cells were purchased from E.H.C. Co. (Japan).

Supporting Information

Supporting Information is available from the Wiley Online Library or from the author.

Acknowledgements

Conflict of Interest

The authors declare no conflict of interest.

Keywords

**ADVANCED
SCIENCE NEWS**

www.advancedsciencenews.com

**ADVANCED
MATERIALS**

www.advmat.de

[1] B. L. Feringa, *Adv. Mater.* **2020**, *32*, 1906416.

[2] I. Aprahamian, *ACS Cent. Sci.* **2020**, *6*, 347.

[3] A. Goulet-Hanssens, F. Eisenreich, S. Hecht, *Adv. Mater.* **2020**, *32*, 1905966.

[4] T. van Leeuwen, A. S. Lubbe, P. Štacko, S. J. Wezenberg, B. L. Feringa, *Nat. Rev. Chem.* **2017**, *1*, 0096.

[5] F. Lancia, A. Ryabchun, N. Katsonis, *Nat. Rev. Chem.* **2019**, *3*, 536.

[6] Q. Li, G. Fuks, E. Moulin, M. Maaloum, M. Rawiso, I. Kulic, J. T. Foy, N. Giuseppone, *Nat. Nanotechnol.* **2015**, *10*, 161.

[7] J. T. Foy, Q. Li, A. Goujon, J. R. Collard-Itté, G. Fuks, E. Moulin, O. Schiffmann, D. Dattler, D. P. Funeriu, N. Giuseppone, *Nat. Nanotechnol.* **2017**, *12*, 540.

[8] J.-R. Colard-Itté, Q. Li, D. Collin, G. Mariani, G. Fuks, E. Moulin, E. Buhler, N. Giuseppone, *Nanoscale* **2019**, *11*, 5197.

[9] J. Berna, D. A. Leigh, M. Lubomska, S. M. Mendoza, E. M. Pérez, P. Rudolf, G. Teobaldi, F. Zerbetto, *Nat. Mater.* **2005**, *4*, 704.

[10] J. Chen, F. K. C. Leung, M. C. Stuart, T. Kajitani, T. Fukushima, E. van der Giessen, B. L. Feringa, *Nat. Chem.* **2018**, *10*, 132.

[11] F. Lancia, A. Ryabchun, A. D. Nguindjel, S. Kwangmettatam, N. Katsonis, *Nat. Commun.* **2019**, *10*, 4819.

[12] T. J. White, D. J. Broer, *Nat. Mater.* **2015**, *14*, 1087.

[13] R. Eelkema, B. L. Feringa, *Org. Biomol. Chem.* **2006**, *4*, 3729.

[14] L. Qin, W. Gu, J. Wei, Y. Yu, *Adv. Mater.* **2018**, *30*, 1704941.

[15] Y. Wang, A. Urbas, Q. Li, *J. Am. Chem. Soc.* **2012**, *134*, 3342.

[16] Y. Wang, Q. Li, *Adv. Mater.* **2012**, *24*, 1926.

[17] N. Katsonis, E. Lacaze, A. Ferrarini, *J. Mater. Chem.* **2012**, *22*, 7088.

[18] Y. Kim, N. Tamaoki, *ChemPhotoChem* **2019**, *3*, 284.

[19] H. K. Bisoyi, Q. Li, *Angew. Chem., Int. Ed.* **2016**, *55*, 2994.

[20] H. K. Bisoyi, Q. Li, *Acc. Chem. Res.* **2014**, *47*, 3184.

[21] Y. Li, C. Xue, M. Wang, A. Urbas, Q. Li, *Angew. Chem., Int. Ed.* **2013**, *52*, 13703.

[22] P. Chen, L. L. Ma, W. Hu, Z. X. Shen, H. K. Bisoyi, S. B. Wu, S. J. Ge, Q. Li, Y. Q. Lu, *Nat. Commun.* **2019**, *10*, 2518.

[23] H. Wang, H. K. Bisoyi, B. X. Li, M. E. McConney, T. J. Bunning, Q. Li, *Angew. Chem., Int. Ed.* **2020**, *59*, 2684.

[24] H. K. Bisoyi, T. J. Bunning, Q. Li, *Adv. Mater.* **2018**, *30*, 1706512.

[25] N. Koumura, R. W. J. Zijlstra, R. A. van Delden, N. Harada, B. L. Feringa, *Nature* **1999**, *401*, 152.

[26] N. P. Huck, W. F. Jager, B. de Lange, B. L. Feringa, *Science* **1996**, *273*, 1686.

[27] A. Bosco, M. G. M. Jongejan, R. Eelkema, N. Katsonis, E. Lacaze, A. Ferrarini, B. L. Feringa, *J. Am. Chem. Soc.* **2008**, *130*, 14615.

[28] R. Eelkema, M. M. Pollard, N. Katsonis, J. Vicario, D. J. Broer, B. L. Feringa, *J. Am. Chem. Soc.* **2006**, *128*, 14397.

[29] R. Eelkema, M. M. Pollard, J. Vicario, N. Katsonis, B. Serrano Ramon, C. W. M. Bastiaansen, D. J. Broer, B. L. Feringa, *Nature* **2006**, *440*, 163.

[30] T. Orlova, F. Lancia, C. Loussert, S. Iamsaard, N. Katsonis, E. Brasselet, *Nat. Nanotechnol.* **2018**, *13*, 304.

[31] F. Lancia, T. Yamamoto, A. Ryabchun, T. Yamaguchi, M. Sano, N. Katsonis, *Nat. Commun.* **2019**, *10*, 5238.

[32] T. Orlova, S. J. Aßhoff, T. Yamaguchi, N. Katsonis, E. Brasselet, *Nat. Commun.* **2015**, *6*, 7603.

[33] T. J. White, S. A. Cazzell, A. S. Freer, D.-K. Yang, L. Sukhomlinova, L. Su, T. Kosa, B. Taheri, T. J. Bunning, *Adv. Mater.* **2011**, *23*, 1389.

[34] A. Ryabchun, A. Bobrovsky, *Adv. Opt. Mater.* **2018**, *6*, 1800335.

[35] M. M. Pollard, M. Klok, D. Pijper, B. L. Feringa, *Adv. Funct. Mater.* **2007**, *17*, 718.

[36] D. Roke, S. J. Wezenberg, B. L. Feringa, *Proc. Natl. Acad. Sci. USA* **2018**, *115*, 9423.

[37] D. Zhao, X. Zhao, J. Wang, H. Peng, Y. Liao, X. Xie, I. I. Smalyukh, Y. Yu, *Macromol. Rapid Commun.* **2019**, *40*, 1900037.

[38] A. Ryabchun, D. Yakovlev, A. Bobrovsky, N. Katsonis, *ACS Appl. Mater. Interfaces* **2019**, *11*, 10895.

[39] C. L. Yuan, W. Huang, Z. G. Zheng, B. Liu, H. K. Bisoyi, Y. Li, D. Shen, Y. Lu, Q. Li, *Sci. Adv.* **2019**, *5*, eaax9501.

[40] H. Wang, H. K. Bisoyi, A. M. Urbas, T. J. Bunning, Q. Li, *J. Am. Chem. Soc.* **2019**, *141*, 8078.

[41] D. Villarón, S. Wezenberg, *Angew. Chem., Int. Ed.* **2020**, *59*, 13192.

[42] Y. Wang, Y. Tian, Y. Z. Chen, L. Y. Niu, L. Z. Wu, C. H. Tung, Q. Z. Yang, R. Boulatov, *Chem. Commun.* **2018**, *54*, 7991.

[43] Q. Z. Yang, Z. Huang, T. J. Kucharski, D. Khvostichenko, J. Chen, R. Boulatov, *Nat. Nanotechnol.* **2009**, *4*, 302.

[44] J. F. Xu, Y. Z. Chen, D. Wu, L. Z. Wu, C. H. Tung, Q. Z. Yang, *Angew. Chem., Int. Ed.* **2013**, *52*, 9738.

[45] N. Zhu, X. Li, Y. Wang, X. Ma, *Dyes Pigm.* **2016**, *125*, 259.

[46] P. G. De Gennes, J. Prost, *The Physics of Liquid Crystals*, Oxford University Press, Oxford **1997**.

[47] D. Katsis, *Liq. Cryst.* **1999**, *26*, 181.

[48] S. H. Chen, D. Katsis, A. W. Schmid, J. C. Mastrangelo, T. Tsutsui, T. N. Blanton, *Nature* **1999**, *397*, 506.

[49] P. R. Gerber, *Z. Naturforsch.* **1980**, *35*, 619.